ELSEVIER

Advances in Colloid and Interface Science 118 (2005) 173 – 190

ADVANCES IN COLLOID AND INTERFACE SCIENCE

www.elsevier.com/locate/cis

Thermodynamic modeling of contact angles on rough, heterogeneous surfaces

J. Long, M.N. Hyder, R.Y.M. Huang, P. Chen *

Department of Chemical Engineering, University of Waterloo, 200 University Ave. W., Waterloo, Ontario, Canada N2L 3G1

Available online 9 September 2005

Abstract

Theoretical modelling for contact angle hysteresis carried out to date has been mostly limited to several idealized surface configurations, either rough or heterogeneous surfaces. This paper presents a preliminary study on the thermodynamics of contact angles on rough and heterogeneous surfaces by employing the principle of minimum free energy and the concept of liquid front. Based on a two-dimensional regular model surface, a set of relations were obtained, which correlate advancing, receding and system equilibrium contact angles to surface topography, roughness and heterogeneity. It was found that system equilibrium contact angles (θ_{ES}) can be expressed as a function of surface roughness factor (δ) and the Cassie contact angle (θ_C): $\cos\theta_{ES}=\delta\cos\theta_C$. This expression can be reduced to the classical Wenzel equation.: $\theta_{ES}=\theta_W$ for rough but homogeneous surfaces, and the classical Cassie equation $\theta_{ES}=\theta_C$ for heterogeneous but smooth surfaces. A non-dimensional parameter called surface feature factor (ω) was proposed to classify surfaces into three categories (types): roughness-dominated, heterogeneity-dominated and mixed-rough-heterogeneous. The prediction of advancing and receding contact angles of a surface is dependent on which category the surface belongs to. The thermodynamic analysis of contact angle hysteresis was further extended from the regular model surface to irregular surfaces; consistent results were obtained. The current model not only agrees well with the models previously studied by other researchers for idealized surfaces, but also explores more possibilities to explain the reported experimental results/observations that most existing theories could not explain.

Keywords: Contact angle hysteresis; Surface modelling; Rough heterogeneous surface; Surafce free energy; Surface thermodynamics

Contents

1. Introduction . . . 174
2. Theory . . . 175
   2.1. The liquid front . . . 175
   2.2. Regular model surface and assumptions . . . 176
   2.3. Changes in system free energy . . . 177
3. Roughness-dominated surfaces . . . 178
4. Heterogeneity-dominated surfaces . . . 179
5. Mixed rough-heterogeneous surfaces . . . 180
6. Surface classification and surface feature factor . . . 181
7. Irregular surfaces . . . 183
   7.1. Roughness-dominated irregular surfaces . . . 183
   7.2. Heterogeneity-dominated irregular surfaces . . . 183
   7.3. Mixed rough-heterogeneous irregular surfaces . . . 183
8. Comparison with experimental results . . . 184

* Corresponding author. Tel.: +1 519 8884567x5586; fax: +1 519 746 4979.
E-mail address: p4chen@cape.uwaterloo.ca (P. Chen).

0001-8686/$ - see front matter © 2005 Elsevier B.V. All rights reserved.
doi:10.1016/j.cis.2005.07.004

9. Conclusions . . . 185
Acknowledgements . . . 186
Appendix A. Validation of the model . . . 186
A.1. Idealized smooth and homogeneous surfaces . . . 186
A.2. Idealized rough but homogeneous surface . . . 187
A.3. Idealized heterogeneous but smooth surface . . . 188
Appendix B. Effect of the Liquid Front Length (H_0) . . . 188
Appendix C. Derivation of the surface feature factor . . . 189
References . . . 190

1. Introduction

Contact angle has been widely used for characterizing interfacial phenomena, including wetting/dewetting of solid surfaces, capillary penetration into porous media, coating and painting. On an ideal solid surface, which is smooth, homogeneous, isotropic and nondeformable, the contact angle is expressed by the well-known Young equation [1]

$$\gamma_{lv}\cos\theta_Y = \gamma_{sv} - \gamma_{sl} \quad (1)$$

where θ_Y is the Young contact angle (also called the intrinsic contact angle, symbolized by θ_e), and γ_{lv}, γ_{sv} and γ_{sl} are the interfacial (surface) tensions of the liquid–vapor, solid–vapor and solid–liquid interfaces, respectively. The Young equation indicates that θ_Y is a unique function of the interfacial tensions, γ_{sv}, γ_{sl}, and γ_{lv}. However, experimentally observed contact angles are not uniquely determined by these interfacial tensions [2]. For real surfaces, there exists a range of contact angles [2,3]; the largest and the smallest among them are termed the advancing contact angle, θ_a, and the receding contact angle, θ_r, respectively. The difference between the advancing and the receding contact angle is the so-called contact angle hysteresis. Surface roughness and heterogeneity as a cause for contact angle hysteresis have been studied by many researchers over the past few decades.

Wenzel [4] first extended the Young Eq. (1) to describing rough surfaces using a surface roughness factor, δ:

$$\gamma_{lv}\cos\theta_w/\delta = \gamma_{sv} - \gamma_{sl} \quad (2)$$

where δ is defined as the ratio of the actual surface area to the geometrically projected area, and θ_w is the Wenzel contact angle. For heterogeneous surfaces, Cassie [5] obtained the following equation for solid surfaces consisting of two domains with intrinsic contact angles, θ_{e1} and θ_{e2}:

$$\cos\theta_C = a_1\cos\theta_{e1} + a_2\cos\theta_{e2} \quad (3)$$

where a_1 and a_2 are the fractional surface areas of the two types of surfaces such that $a_1+a_2=1$, and θ_C is the Cassie contact angle, the equilibrium contact angle for heterogeneous but smooth solid surfaces.

Shuttleworth and Bailey [6] and Johnson and Dettre [7,8] developed surface models that provided the first quantitative results linking contact angle hysteresis to surface heterogeneity and roughness. Later, Neumann and Good [3] and Eick et al. [9] developed a contact angle model for smooth but heterogeneous vertical plates; they demonstrated the existence of a large number of metastable states. A fundamental study by Huh and Mason [10] also revealed the effect of surface roughness on wetting, where they considered a liquid drop growing or retracting concentrically on a solid surface with axisymmetric grooves. In the early 1980s, Oliver and Mason [11] showed that wetting hysteresis occurs on all surfaces, exceeding the range predicted theoretically from roughness measurements made by surface profilometry.

All these early models of contact angle hysteresis on solid surfaces assumed the surface to be either smooth (flat) or heterogeneous (chemically), but not to be both. Moreover, these models considered simple, periodic modulations of surface profiles, such as parallel or axisymmetric grooves. However, real surfaces are often irregular in shape. In the mid 1980s, Joanny and de Gennes [12] and Robbins and Joanny [13] developed a model for contact angle hysteresis of solid surfaces that had non-periodic profiles. The model was developed for weakly or strongly heterogeneous surfaces and able to predict contact angle hysteresis using the concept of pinning of three-phase contact lines by surface impurities and existence of metastable states. Recently, Marmur and co-workers [14–18] proposed a model for 2-D (cylindrical) drops on a periodically heterogeneous but smooth solid surface. Their calculations revealed a possibility of the dependence of advancing and receding contact angles on the drop volume. In 2002, a model by Extrand [19] for rough and ultrahydrophobic surfaces showed that contact angle hysteresis is independent of absolute values of surface roughness, but the surface asperity shape and linear fraction of the contact line. Öpik [20] also studied contact angle hysteresis by considering a random distribution of weak heterogeneities on a solid surface. Based on a probability analysis, he proposed a model that could show contact angle hysteresis to arise as a result of a random distribution of irregularities (heterogeneities) of the surface.

Except for surface roughness and heterogeneity, there are other factors that may cause contact angle hysteresis. Lam and co-workers [21–23] considered liquid absorption and/or retention (swelling) to be responsible for the hysteresis that they observed on smooth surfaces of polymer films. They found [22] that "Models ascribing contact angle hysteresis to features of the solid surface such as roughness and heterogeneity may well be applicable in certain situations, but not on carefully prepared films of polymeric materials". In a

Chilbowski's paper [24], contact angle hysteresis is considered to be due to the liquid film left behind the drop during the contact line retracting. Also, there are studies, e.g., Decker et al. [25] and Gouin [26,27], indicating that the three-phase contact line imposes an impact on contact angle hysteresis. These studies indicate that contact angle hysteresis is a very complicated phenomenon and many factors can play a role. In the present study, we focus on the effect of surface roughness and heterogeneity on contact angle hysteresis and limit our scope of modelling to the case where no liquid film is present and no adsorption occurs. Contact angle hysteresis could also arise from molecular rearrangements occurring at solid–liquid interfaces after they have come into contact [28].

From the above review, we find that research on contact angle phenomena has been active. Various researchers have studied the effect of roughness or heterogeneity on contact angles with model surfaces of regular or periodic distribution patterns [3–11] and, in some cases, with weakly or strongly heterogeneous surfaces [12,13] without a periodic pattern. Each model seems to be developed for a specific type of surface. To date, there has been no model available for contact angle hysteresis on mixed rough-heterogeneous surfaces where the effects of roughness and heterogeneity are equally important. Until now, there has been no treatment that gives quantitative relations between contact angle hysteresis and surface topography/heterogeneity for rough, heterogeneous surfaces. In this study, we made a preliminary attempt to develop a thermodynamic treatment for rough, heterogeneous surfaces. A two-dimensional regular rough-heterogeneous model surface was proposed. A set of quantitative relations that correlate advancing, receding and system equilibrium contact angles to surface topography and heterogeneity were obtained. The expression for system equilibrium contact angles can be reduced to the Wenzel equation for rough but homogeneous surfaces, and to the Cassie equation for heterogeneous but smooth surfaces. The proposed regular model surface was further extended to two-dimensional irregular surfaces.

Because different sets of contact angle equations apply to different surfaces, in order to classify different types of surfaces, we propose a surface feature factor (ω) to divide surfaces into three categories: roughness-dominated, heterogeneity-dominated, and mixed rough-heterogeneous surfaces. Physically, this new surface feature factor represents competition between surface roughness and surface heterogeneity in affecting contact angles. For a smooth surface, $\omega=0$. For a homogeneous surface, $\omega=\infty$. In the case of mixed rough-heterogeneous surfaces, $0.2<\omega<2$. This non-dimensional factor may be used in classifying surfaces just like the Reynold's number in characterizing fluid flow patterns.

2. Theory

The complexity of contact angles on rough, heterogeneous surfaces is twofold. First, these surfaces themselves are complicated in terms of surface configuration; both surface roughness and heterogeneity have to be taken into consideration. Second, the effect of liquid menisci and gravity on the system free energy is complicated. When a liquid forms a contact angle on a solid surface, the meniscus of the liquid is controlled by the Laplace equation of capillarity, which is a non-linear differential equation, difficult to solve. Only the vertical plate model of Neumann and coworkers [2,3,9] treats the menisci using the Laplace equation and takes the effect of gravity into consideration. Other models, e.g., the sessile drop model of Marmur [14], consider the profile of a sessile drop as a spherical cap, and neglect the effect of gravity. In order to study the thermodynamics of contact angles on rough, heterogeneous surfaces, certain assumptions must also be made. In this section, we first introduce the concept of liquid front, followed by proposing a model rough, heterogeneous surface. Assumptions are then made for the thermodynamic treatments. Finally, the equations that relate the change in system free energy to macroscopic/apparent contact angle are derived.

2.1. The liquid front

When a sessile drop, sitting on a horizontal solid surface, spreads from a state with a contact angle θ to an adjacent one with a contact angle $\theta+\Delta\theta$, as shown in Fig. 1 (left), the free energy of the system will change due to (1) a change in solid–vapor interfacial area and a corresponding change in solid–liquid interfacial area, (2) a change in liquid–vapor interfacial area, and (3) the work which has to be done against gravity for such a change in configuration. The first change can be easily determined by the position of the three-phase contact line. The second change is directly related to the liquid meniscus. It is very difficult to determine the exact change in liquid–vapor interfacial area (or liquid surface area), particularly for complicated surfaces such as those on rough-heterogeneous solid surfaces. The free energy change due to the work done against gravity is also difficult to be calculated. As a result, the effect of gravity is often neglected.

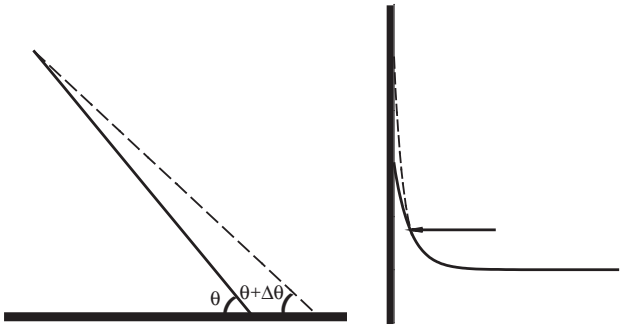

Fig. 1. A demonstration of liquid front. Left drawing represents a sessile drop sitting on a horizontal solid surface. Right drawing is the cases of a vertical plate partially immersed in a fluid.

In order to determine the change in liquid surface area, simplification/approximation must be made. In general, the size of a sessile drop is much larger than the scale of surface roughness and heterogeneity. As shown in Fig. 1 (left), the liquid front, from the three-phase contact point up to a certain point on the liquid surface, can therefore be regarded as a straight line. This treatment can be more clearly illustrated by the case of a vertical plate immersed in a liquid, Fig. 1 (right), which shows that the liquid front, from the point indicated by the arrow to the three-phase contact point, can be approximated as a straight line. As the liquid front moving from one state with a contact angle θ to an adjacent one with a contact angle $\theta+\Delta\theta$ has little effect on the bulk liquid, the free energy change of the entire system can be assumed to be mainly determined by the interfacial area changes nearby the three-phase contact line. The free energy change of the system due to the change of liquid surface area can be determined by the movement of the liquid front. This makes the free energy calculation and the modelling of complicated (such as rough-heterogeneous) surfaces possible. The concept of liquid front, in fact, was previously adopted to derive the Young equation [29], although it was not explicitly defined in the present way.

2.2. Regular model surface and assumptions

The regular rough, heterogeneous model surface proposed is shown in Fig. 2. It is a two-dimensional model, which means all parameters will not change in the z direction or the direction normal to the plane of the paper. This surface consists of alternating material strips indicated by black and grey segments, respectively. The widths of the two strips may not be equal. Each material strip has its own intrinsic contact angle. Therefore, the intrinsic contact angle may change along the x direction at different surface spots and can be generally described as a function of x,

$$\theta_e = \theta_e(x). \tag{4}$$

The surface heterogeneity of this model can be extended from two materials to three or more materials if necessary. With respect to surface roughness, trapezoids are used to represent the surface profile. Such a trapezoidal surface configuration is a rather general geometry and can be reduced to various simpler surface configurations as shown in Fig. 3. At any point of the surface, the height of a surface spot, y, can be expressed as a function of x:

$$y = y(x). \tag{5}$$

For a two-dimensional (cylindrical) sessile drop sitting on such a model surface, the following assumptions are made in order to calculate the free energy change of the system:

(1) A liquid front exists and is of a straight line. The movement of the liquid front and hence interfacial area changes determine the free energy change of the entire system.
(2) Gravity is negligible. On a horizontal solid surface, this assumption is reasonable as the gravity centre of the liquid drop will not change significantly as a result of the liquid front movement. This assumption has been used in most of the previous models [7,8,14].

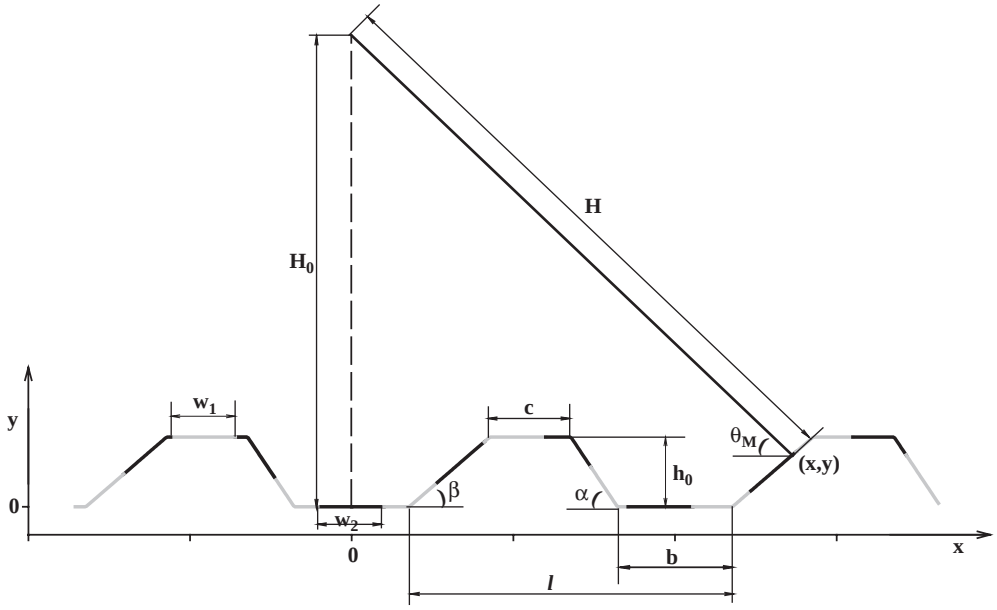

Fig. 2. A cross-sectional view of the model rough and heterogeneous surface. l: length of a repeated roughness unit containing a trapezoidal bump. h_0: height of the bump. c: length of the top side of the bump. b: length of the smooth portion of a repeat unit. α,β: geometric angles of the trapezoid. H_0: initial height of the liquid front. H: length of the liquid front at any location. θ_M: macroscopic/apparent contact angle. The black and grey segments represent different materials on the surface. w_1, w_2: the length of a black and a grey segment.

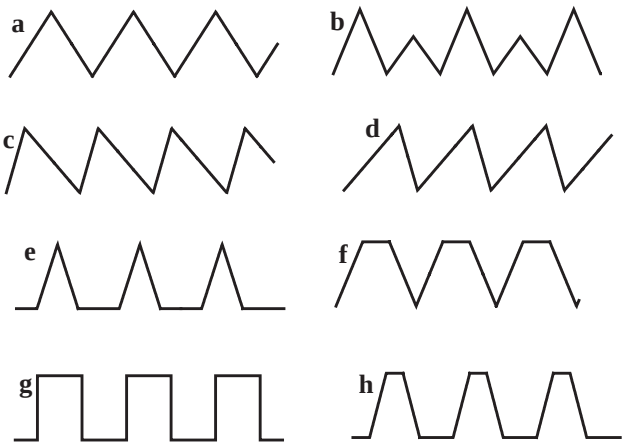

Fig. 3. Some specific surface configurations that can be derived from the model surface shown in Fig 2. a — isosceles triangles ($c=b=0$, $\alpha=\beta$); b — isosceles triangles with varying h_0; c — triangles ($c=b=0$, $\alpha<\beta$); d — triangles ($c=b=0$, $\alpha>\beta$); e — triangles ($c=0$, $b\neq 0$, $\alpha=\beta$); f — isosceles trapezoids ($c\neq 0$, $b=0$, $\alpha=\beta$); g — rectangles ($\alpha=\beta=90°$); h — isosceles trapezoids ($\alpha=\beta$).

(3) There is no effect of line tension as this is a two-dimensional model and the three-phase contact line is a straight line. In fact, even if the sessile drop is three-dimensional, the line tension is extremely small and thus can be neglected for a macroscopic drop [30].
(4) The Young equation is locally valid. This assumption is essentially correct and has been obtained as a result by the model of Li and Neumann [2]. It is also proved to be correct by Wolansky and Marmur [31] if line tension can be ignored.
(5) The solid surface itself is undeformable and rigid and there is no liquid film existing in front of the three-phase contact line.

2.3. Changes in system free energy

When the liquid front moves from the reference state to an adjacent configuration, the total free energy of the system will change due to changes in solid–vapor/solid–liquid interfacial area and liquid–vapor interfacial area. The system free energy change (ΔF) can be given by

$$\Delta F = \Delta F_1 + \Delta F_2 \tag{6}$$

where ΔF_1 is the free energy change due to the change in solid–vapor interfacial area and the corresponding change in solid–liquid interfacial area, and ΔF_2 is the free energy change due to a change in liquid–vapor interfacial area.

ΔF_1 is the driving force term, which represents the work done on the system in replacing the solid–vapor interface (of interfacial free energy, γ_{sv}) with the solid–liquid interface (of interfacial free energy, γ_{sl}):

$$\mathrm{d}(\Delta F_1) = -L(\gamma_{sv}-\gamma_{sl})\mathrm{d}s \tag{7}$$

where L is the liquid front width, and s is the topographic length of the (rough) surface, which is a function of x.

The Young equation is locally valid:

$$\gamma_{lv}\cos\theta_e = \gamma_{sv} - \gamma_{sl} \tag{8}$$

where θ_e is the local intrinsic contact angle, which is a function of x or s (the topographic length of the real surface starting from the origin). Combining Eqs. (4), (7) and (8 gives

$$\Delta F_1 = \int_0^s -L\gamma_{lv}\cos\theta_e(x)\mathrm{d}s. \tag{9}$$

The term ΔF_2 is the work done on the system for expanding the liquid surface:

$$\Delta F_2 = L\gamma_{lv}\Delta H \tag{10}$$

where γ_{lv} is the interfacial free energy (tension) of liquid–vapor, and ΔH is the increase in liquid front length:

$$\Delta H = H - H_0 = \sqrt{(H_0-y)^2+x^2} - H_0 \tag{11}$$

Combining Eqs. (10) and (11) gives

$$\Delta F_2 = L\gamma_{lv}\left(\sqrt{(H_0-y)^2+x^2} - H_0\right) \tag{12}$$

From Eqs. (6), (9) and (12) the system free energy change can be expressed by

$$\Delta F = \int_0^s -L\gamma_{lv}\cos\theta_e(x)\mathrm{d}s + L\gamma_{lv}\left(\sqrt{(H_0-y)^2+x^2} - H_0\right) \tag{13}$$

To correlate the system free energy change with the macroscopic/apparent contact angle, θ_M, the following geometric relation can be employed:

$$\tan\theta_M = \frac{H_0-y}{x} \tag{14}$$

Combining Eqs. (4), (5), (13) and (14), the system free energy change as a function of the macroscopic contact angle can be calculated. A Java program has been written to implement all the calculations presented in this paper. In all calculations, we set $L=1$ m and $\gamma_{lv}=72.6$ mJ/m^2 (water surface tension at room temperature) for convenience.

To validate this model, the system free energy change for several specific surfaces studied by Neumann and co-workers [2,3,9], including the idealized, smooth and homogeneous surface, the idealized rough but homogeneous surface, and the idealized heterogeneous but smooth surface, were computed. Details can be found in Appendix A. The results show that this model agrees with all existing models for these specific surfaces. In addition, in all the calculations of free energy, a chosen H_0 much larger than the size of surface roughness or heterogeneity unit was used. It was found in fact that advancing and receding contact angles are not affected by H_0 even if H_0 is close to the size of a roughness peak. However, system equilibrium angles are

greatly affected by the value of H_0. To obtain a system equilibrium angle close to the theoretically predicted value, a H_0 much larger than the size of the roughness peaks (e.g., $5 \sim 10$ times larger) must be used. A detailed discussion on the effect of H_0 is given in Appendix B.

In the following, the proposed model is applied to more general surfaces, being both rough and heterogeneous. The subsequent three sections will, respectively, present the results for three types of rough, heterogeneous surfaces: roughness-dominated, heterogeneity-dominated, and mixed rough-heterogeneous surfaces.

3. Roughness-dominated surfaces

For rough, heterogeneous surfaces, if the characteristic size of surface heterogeneity, e.g., the strip width of alternating surface materials, is much smaller than the characteristic size of roughness, e.g., the width or height of the bump (Fig. 2), such surfaces can be considered to be roughness-dominated. An applicable parameter will be defined in Section 6 to determine if a surface is roughness-dominated. Let l=200 μm, c=50 μm, h_0=30 μm, β=30°, α=45°, θ_{e1}=50°, θ_{e2}=70°, w_1=10 μm, w_2=10 μm, and H_0=1600 μm (see Fig. 2 and the Nomenclature for the symbols used). In this case, the length of a bump, l, is 10 times the width of the two materials, w_1+w_2. The system free energy change as a function of the macroscopic contact angle for such a roughness-dominated surface is shown in Fig. 4.

The shape of energy barriers in Fig. 4 is similar to the shape of the surface bumps shown in Fig. 2. This finding indicates that the energy barriers are mainly determined by the surface roughness or topography. However, as shown in the inset in Fig. 4, each major energy barrier, e.g., from point 1 to point 5, itself includes many small energy barriers. These small energy barriers result from the weak heterogeneity of the surface. To overcome a major energy barrier, for example, from point 1 to point 5, the energy needed is 1.8×10^{-6} J. To overcome a small energy barrier, e.g., from point 1 to point 3, the energy required is 1.2×10^{-7} J. These results indicate that the energy required to overcome a major energy barrier is around 15 times that to overcome a small energy barrier. Therefore, the measurable contact angles of the system, e.g., advancing and receding contact angles, will be determined mainly by the major energy barriers. The free energy curve also shows that there are a number of metastable equilibrium configurations or local minima within the contact angle range from 30.5° to 105.5°. The limiting angles, corresponding to the first and the last local minima, represent the receding and advancing contact angles of the system. There is a global minimum for the system at θ_M=55.08°. This angle is the so-called system equilibrium contact angle, θ_{ES}.

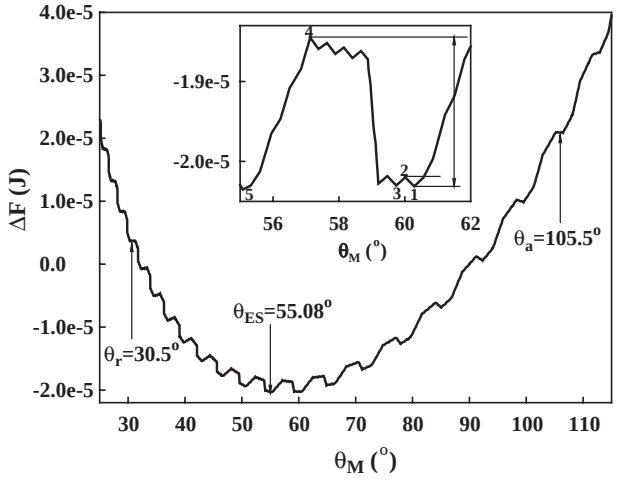

Fig. 4. Free energy change as a function of macroscopic contact angle for a roughness-dominated surface. l=200 μm (>w_1, w_2), c=50 μm, h_0=30 μm, β=30°, α=45°, θ_{e1}=50°, θ_{e2}=70°, w_1=w_2=10 μm, δ=1.1023, H_0=1600 μm.

Analysing and summarising the results discussed above give the following relations for roughness-dominated surfaces:

$$\theta_a = \theta_C + \alpha \tag{15}$$

$$\theta_r = \theta_C - \beta \tag{16}$$

$$\cos\theta_{ES} = \delta\cos\theta_C \tag{17}$$

These equations can also be mathematically obtained from the equations alone. As the strip width is much smaller than the size of the rough bump, using the Cassie equation, Eq. (13) can be approximated by

$$\Delta F = -L\gamma_{lv}\cos\theta_C \cdot s(x) + L\gamma_{lv}\left(\sqrt{(H_0 - y)^2 + x^2} - H_0\right) \tag{18}$$

Differentiating ΔF gives

$$\frac{d\Delta F}{dx} = -L\gamma_{lv}\cos\theta_C \cdot \frac{ds}{dx} - L\gamma_{lv}\sin\theta_M \frac{dy}{dx} + L\gamma_{lv}\cos\theta_M \tag{19}$$

The model surface configuration (Fig. 2) shows that the possible values of dy/dx and ds/dx include 0 and 1, $\tan\beta$ and $1/\cos\beta$, and $-\tan\alpha$ and $1/\cos\alpha$. Substituting these values for dy/dx and ds/dx in Eq. (19), three values of θ_M will satisfy $d\Delta F/dx = 0$:

$$\theta_M = \theta_C \tag{20}$$

$$\theta_M = \theta_C + \alpha \tag{21}$$

$$\theta_M = \theta_C - \beta \tag{22}$$

The two θ_Ms in Eqs. (21) and (22) represent two local minima of the free energy curve, corresponding to the advancing (θ_a) and receding (θ_r) contact angles. Eqs. (21) and (22) are in fact Eqs. (15) and (16). As for θ_M in Eq.

(20), its value is between θ_r and $\theta_{a;}$ on a free energy curve, there is possibly a local minimum or maximum at which Eq. (20) is satisfied.

If the surface under investigation is a rough but homogeneous surface, then Eqs. (15) and (16) will reduce to the forms first derived by Shuttleworth and Bailey (30): $\theta_a=\theta_e+\alpha$ and $\theta_r=\theta_e-\beta$. Furthermore, if the surface has symmetric peaks, then $\alpha=\beta$ and thus, $\theta_a=\theta_e+\alpha$ and $\theta_r=\theta_e+\alpha$, which have been widely explored by many investigators ((8), (22), (30)–(34)).

To obtain the global minimum or the system equilibrium contact angle, Eq. (18) can be further approximate under the condition that H_0 is large enough such that

$$\Delta F = -L\gamma_{lv}\cos\theta_C\cdot\delta\cdot x + L\gamma_{lv}\left(\sqrt{H_0^2+x^2}-H_0\right) \quad (23)$$

By satisfying $d\Delta F/dx=0$, the following relation can be obtained:

$$\cos\theta_M = \delta\cos\theta_C, \quad (24)$$

which is Eq. (17); θ_M in Eq. (24) represents the system equilibrium contact angle.

Because $|\cos\theta_M|$ is always less than or equal to 1, if $|\delta\cos\theta_C|$ in Eq. (17) or Eq. (24) is greater than 1, the system will not have an equilibrium contact angle, or will have an equilibrium contact angle of zero. This conclusion may have an important practical application: by increasing surface roughness, one can always have complete wetting on the surface—an ultra-hydrophilic surface, regardless of the surface material. In addition, Eq. (22) or Eq. (16) also indicates that the receding contact angle will be negative if $\theta_C<\beta$. In this situation, the system will not have a receding contact angle, or the receding contact angle equals zero.

4. Heterogeneity-dominated surfaces

In the above section, we have presented and discussed the results for a typical roughness-dominated surface. If the characteristic size of heterogeneity of a surface is much larger than the characteristic size of roughness, such a surface is heterogeneity-dominated. A typical free energy curve as a function of macroscopic contact angle for a heterogeneity-dominated surface is shown in Fig. 5a. The surface configuration is shown in Fig. 2 with $w_1=w_2=100$ μm and $l=10$ μm, where $(w_1+w_2)/l=20$; other parameters are $c=2$ μm, $h_0=1.5$ μm ($<w_1$, w_2), $\beta=20°$, $\alpha=30°$, $\theta_{e1}=50°$, $\theta_{e2}=70°$, $\delta=1.0666$, and $\theta_C=60.5°$. Fig. 5a shows that the free energy curve has a saw-toothed structure, which is similar to that of an idealized heterogeneous surface (see Fig. A1-3 in Appendix A). This curve gives $\theta_a=68.6°$ and $\theta_r=46.72°$. Obviously, the two values do not satisfy Eqs. (15) and (16). Based on a large number of calculations for different cases, θ_a and θ_r on such

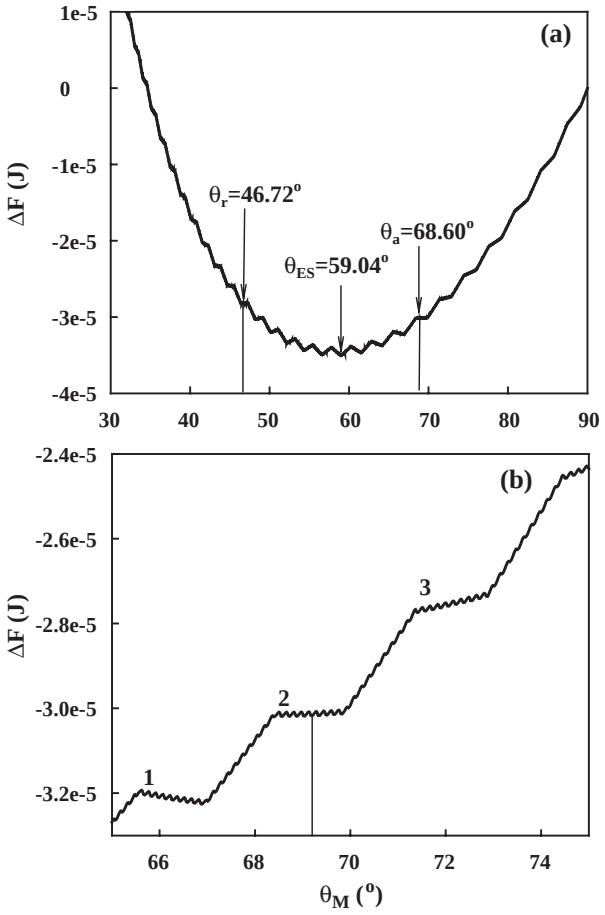

Fig. 5. Free energy change as a function of macroscopic contact angle for a heterogeneity-dominated surface with $H_0=3200$ μm, $l=10$ μm ($<w_1$, w_2), $c=2$ μm, $h_0=1.5$ μm, $\beta=20°$, $\alpha=30°$, $\theta_{e1}=50°$, $\theta_{e2}=70°$, $w_1=w_2=100$ μm. $\theta_C=60.5°$. $\delta=1.0666$, $\theta_{ES}=58.32°$. (b) is part of (a) but on a much smaller scale.

heterogeneity-dominated surfaces were found to satisfy the following relations:

$$\cos\theta_a = \delta\cos(\theta_e)_{max} \quad (25)$$

$$\cos\theta_r = \delta\cos(\theta_e)_{min} \quad (26)$$

where $(\theta_e)_{max}$ and $(\theta_e)_{min}$ represent the maximum and minimum intrinsic contact angles, respectively, i.e., $(\theta_e)_{max}=\theta_{e2}=70°$ and $(\theta_e)_{min}=\theta_{e1}=50°$ as shown Fig. 5. The curve in Fig. 5a also gives the system equilibrium contact angle $\theta_{ES}=59.04°$. This value is close to the one calculated from Eq. (17), 58.32°. This indicates that for heterogeneity-dominated surfaces, the system equilibrium contact angle still satisfies Eq. (17). Another worth-noting point is that each line segment of the saw-toothed structure shown in Fig. 5a appears smooth. However, as shown by the curve on a smaller scale in Fig. 5b, each line segment in fact contains a number of small steps. Because the surface is heterogeneity-dominated, it is reasonable to conclude that the saw-toothed structure (Fig. 5a) results from the heterogeneity and that the small steps (Fig. 5b) come from the roughness.

Fig. 5b also shows more local minima than those shown in Fig. 5a. However, not all the local minima in Fig. 5b can be observed as a metastable state. This is because the energy barrier produced by such small steps is too small. For example, if the system is in a state of stage 3 (Fig 5b), it is very easy for the system to overcome the energy barrier and to move to the adjacent state on its left side with a lower free energy (One of the common driving forces for this process is thermal fluctuations.) This procedure will continue until the system comes to a state in stage 2. Within stage 2, the local minimum at which $\theta_M=68.6°$ has the lowest free energy when comparing to its adjacent states. This point may represent a metastable state, and correspond to the advancing contact angle of the system. If the system is at a local minimum in stage 1, the system will move towards its right side until the lowest free energy point in stage 1. This point represents another metastable state that can be seen in Fig. 5a.

Eqs. (25) and (26) can also be derived from the free energy equations alone. The procedure is as follows: Because the surface is heterogeneity-dominated, the size of rough bumps is small, $s(x)$ can be approximated as $s(x)\approx\delta' x$. In addition, the height of the bump is also quite small comparing with H_0, as a result, $H_0-y\approx H_0$. Thus, Eq. (13) can be simplified as

$$\Delta F=\int_0^x -L\gamma_{lv}\cos\theta_e(x)\delta \mathrm{d}x+L\gamma_{lv}\left(\sqrt{H_0^2+x^2}-H_0\right). \tag{27}$$

Differentiating ΔF gives $\mathrm{d}\Delta F/\mathrm{d}x=-L\gamma_{lv}\delta\cos\theta_e(x)+L\gamma_{lv}\cos\theta_M$. As $\theta_e(x)$ can only be one of the two intrinsic contact angles, two possible macroscopic contact angles satisfying Eqs. (25) and (26) can be obtained by setting $\mathrm{d}\Delta F/\mathrm{d}x=0$.

5. Mixed rough-heterogeneous surfaces

In the preceding sections, we have discussed two special types of rough, heterogeneous surfaces: roughness-dominated and heterogeneity-dominated. However, if the characteristic size of heterogeneity of a surface is neither much smaller nor much greater than the characteristic size of its roughness, we would have a mixed rough-heterogeneous surface. In this section we present and discuss the results of this type of surfaces in detail.

Fig. 6 shows a typical free energy curve for a general rough, heterogeneous surface. The surface configuration used for this figure is the general one shown in Fig. 2. In this case, the length of a roughness unit is $l=100$ μm (the corresponding surface length $L_r=112.72$ μm) and the length of a heterogeneity unit, L_h, is 200 μm ($L_h=w_1+w_2$). Although the shape of the free energy curve in Fig. 6 shows irregularity, some common features from this curve can be found when compared with other free energy curves

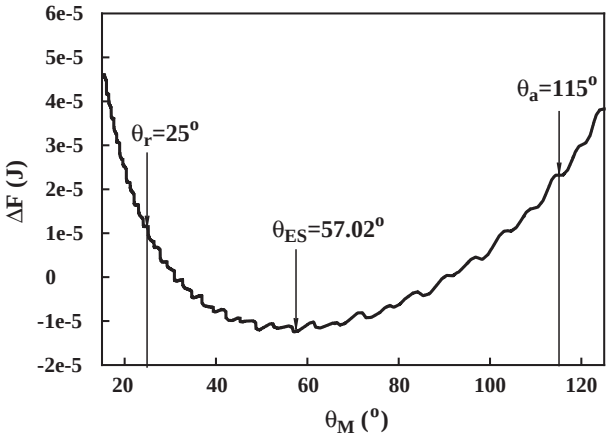

Fig. 6. The free energy change as a function of macroscopic contact angle for a mixed rough, heterogeneous surface: $l=100$ μm ($\sim w_1$, w_2), $c=20$ μm, $h_0=20$ μm, $\alpha=45°$, $\beta=25°$, $w_1=w_2=100$ μm, $\theta_{e1}=50°$, $\theta_{e2}=70°$, $H_0=900$ μm, $\delta=1.2728$, $\theta_C=60.5°$.

discussed above. First, there are two plateaus (of a zero slope) appearing on two sides of the curve. The left one is at $\theta_M=25°$, and the right one is at $\theta_M=115°$. Between these two values, there are a number of local minima, which correspond to metastable states of the system. When θ_M is less than 25° or greater than 115°, there is no local minima any more. This indicates that 25° and 115° are the minimum and maximum contact angles among possible contact angles of the system. The two angles thus represent the receding and the advancing contact angle, respectively, which can be evaluated by

$$\theta_a=(\theta_e)_{\max}+\alpha \tag{28}$$

$$\theta_r=(\theta_e)_{\min}-\beta \tag{29}$$

These two equations can also be derived from the free energy equations. Differentiating Eq. (13) gives

$$\frac{\mathrm{d}\Delta F}{\mathrm{d}x}=-L\gamma_{lv}\cos\theta_e(x)\frac{\mathrm{d}s}{\mathrm{d}x}-L\gamma_{lv}\sin\theta_M\frac{\mathrm{d}y}{\mathrm{d}x}+L\gamma_{lv}\cos\theta_M \tag{30}$$

For a general surface configuration shown in Fig. 2, there are six possible combinations of $\theta_e(x)$, $\mathrm{d}y/\mathrm{d}x$ and $\mathrm{d}s/\mathrm{d}x$. These are (θ_{e1}, $\tan\beta$, $1/\cos\beta$), (θ_{e2}, $\tan\beta$, $1/\cos\beta$), (θ_{e1}, $-\tan\alpha$, $1/\cos\alpha$), (θ_{e2}, $-\tan\alpha$, $1/\cos\alpha$), (θ_{e1}, 0, 1), and (θ_{e2}, 0, 1). Substituting for $\theta_e(x)$, $\mathrm{d}y/\mathrm{d}x$ and $\mathrm{d}s/\mathrm{d}x$ in Eq. (30) with the six groups of values and setting $\mathrm{d}\Delta F/\mathrm{d}x=0$, six possible values of θ_M are obtained: $\theta_{e1}-\beta$, $\theta_{e2}-\beta$, $\theta_{e1}+\alpha$, $\theta_{e2}+\alpha$, θ_{e1}, and θ_{e2}. In the six values, the maximum and minimum ones will represent the advancing and the receding contact angles of the system. Thus, Eqs. (28) and (29) are obtained.

The free energy curve in Fig. 6 also gives the system equilibrium contact angle, $\theta_{ES}=57.02°$. With $\delta=1.2728$ and $\theta_C=60.5°$, the calculated value of θ_{ES} from Eq. (17) is 56.29°. The two θ_{ES} values are close; thus, Eq. (17) is still

valid for mixed rough-heterogeneous surfaces. In fact, Eq. (17) can also be derived from Eq. (13) for mixed rough-heterogeneous surfaces. The derivation is the same as that for roughness-dominated surfaces (Eqs. (18), (23) and (24)).

6. Surface classification and surface feature factor

In the above three sections, we have discussed three types of rough and heterogeneous surfaces: roughness-dominated, heterogeneity-dominated, and mixed rough-heterogeneous surfaces. Although qualitative descriptions about the three types of surfaces have been provided, quantitatively distinguishing them is desired. The results presented in the preceding three sections show that the three types of surfaces produce different advancing and receding contact angles. Therefore, it is important to know which type a surface under study belongs to.

Advancing and receding contact angles are the maximum and minimum among metastable state contact angles. On a free energy curve, the receding and advancing contact angles correspond to the first and the last local minima, respectively. Eq. (6) shows that the free energy change (ΔF) consists of two terms. One is due to changes in solid–vapor and solid–liquid interfacial areas (ΔF_1), and the other due to a change in liquid–vapor interfacial area (ΔF_2). As expressed by Eq. (9), ΔF_1 is related to surface heterogeneity, whereas ΔF_2 is directly related to surface roughness but independent of surface heterogeneous, see Eq. (12). Therefore, ΔF_1 represents the contribution of surface heterogeneity to ΔF, while ΔF_2 represents the contribution of surface roughness to ΔF. Thus, the classification of surfaces may be made by comparing ΔF_1 and ΔF_2.

Eqs. (9), (12) and (13) can be used to calculate ΔF_1, ΔF_2, and ΔF, respectively. Fig. 7 presents several groups of the results. The surface configuration used in Fig. 7 is the one with isosceles triangles shown in Fig. 3a. To focus on the effect of surface heterogeneity on ΔF_1 the surface length $s(x)$, instead of x, is used as the horizontal coordinate in Fig. 7. Fig. 7a is a case of the heterogeneity-dominated surface. The three curves show that the curve of ΔF_1 has a saw-toothed structure, while the curve of ΔF_2 is almost smooth. The shape and the major steps of the ΔF curve are determined by ΔF_1. The minor steps of the ΔF curve are due to ΔF_2. Fig. 7b is a case of the roughness-dominated surface. In this case, ΔF_2 determines the shape and the major steps of the ΔF curve, whereas ΔF_1 determines the minor steps of the ΔF curve. Fig. 7c presents the results of a mixed rough-heterogeneous surface. In this case, the shape of the ΔF curve is quite irregular and is determined by a combination of ΔF_1 and ΔF_2.

Fig. 8 gives a close look of Fig. 7c around $s=0$. The grey, dash-dotted, and solid lines in Fig. 8 represent the curves of ΔF_1, ΔF_2 and ΔF, respectively. At $s=0$ (point A),

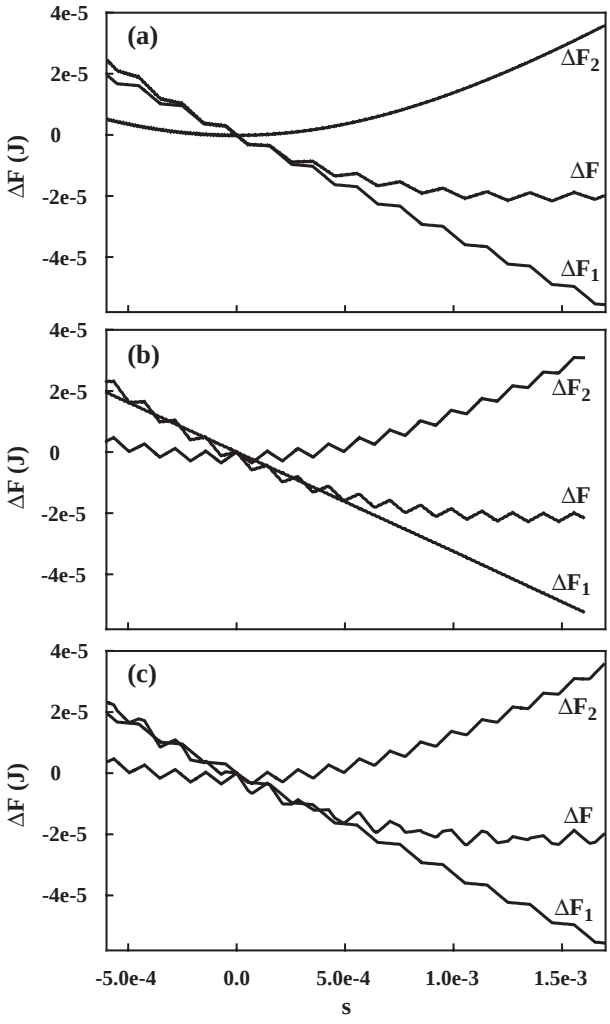

Fig. 7. The contribution of ΔF_1 and ΔF_2 to ΔF. (a) a heterogeneity-dominated surface: $l=10$ μm ($\ll w_1$, w_2), $c=0$ μm, $h_0=5$ μm, $\alpha=\beta=45°$, $w_1=w_2=100$ μm, $\theta_{e1}=35°$, $\theta_{e2}=85°$, $H_0=1200$ μm. (b) a roughness-dominated surface: $l=100$ μm ($\gg w_1$, w_2), $c=0$ μm, $h_0=50$ μm, $\alpha=\beta=45°$, $w_1=w_2=10$ μm, $\theta_{e1}=35°$, $\theta_{e2}=85°$, $H_0=1200$ μm. (c) a mixed rough-heterogeneous surface: $l=100$ μm ($\sim w_1$, w_2), $c=0$ μm, $h_0=50$ μm, $\alpha=\beta=45°$, $w_1=w_2=100$ μm, $\theta_{e1}=35°$, $\theta_{e2}=85°$, $H_0=1200$ μm. The surface configuration is shown in Fig. 3a.

the liquid front is at the reference state ($\theta_M=90°$). When the liquid front moves and goes to the next peak, ΔF_2 changes along curve ACB. If the liquid front moved over the same distance as the surface length to the peak (L_r) on a smooth surface, ΔF_2 would change along the dotted straight line, from point A to point B. Thus the area of the triangle ABC, S_{ABC}, represents the free energy difference between the two paths. Similarly, when the liquid front moves from a state, e.g., point a, through a heterogeneity unit to point B, ΔF_1 will change along curve acb. The dotted straight line ab would represent the path of ΔF_1 if the surface were homogeneous. The area of triangle abc, S_{abc}, represent the free energy difference between the two paths: imaginary and real. Therefore, we propose a parameter using these two triangle areas, i.e., $\sqrt{\frac{S_{ABC}}{S_{abc}}}$, for comparing the contributions of

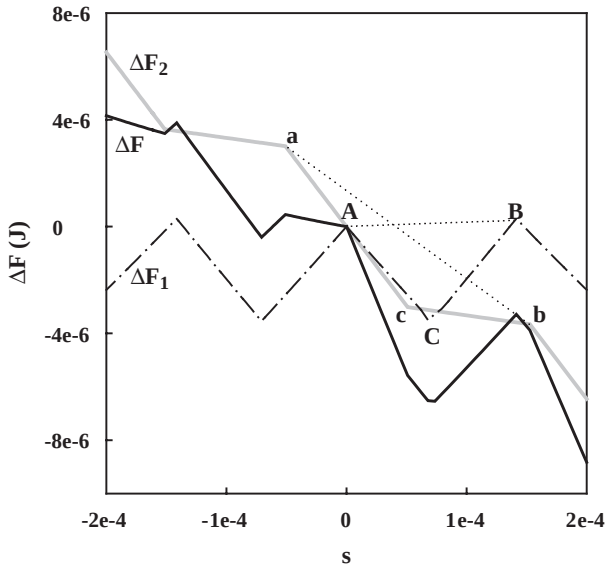

Fig. 8. A close look of Fig. 7c around $s=0$ to determine the surface feature factor from ΔF_1 and ΔF_2. Starting at $s=0$ (point A), when the liquid front goes over a peak, ΔF_2 changes along the dot–dash curve ACB until point B. If the liquid front moves over the same distance on a smooth surface, ΔF_2 will change along the dotted straight line from point A to point B. Thus the area of the triangle ABC, S_{ABC}, represents the "sum" of free energy difference between the two paths. Similarly, when the liquid front moves from a state, e.g., point a through a heterogeneity unit to point b, ΔF_1 will change along the grey curve acb. The dotted straight line ab represents the change track of ΔF_1 if the surface is homogeneous. The area of triangle abc, S_{abc}, represent the "sum" of free energy difference between the two paths. The surface feature factor is then obtained by $= \sqrt{\frac{S_{ABC}}{S_{abc}}}$.

ΔF_2 and ΔF_1 to ΔF. This parameter may be named the surface feature factor, ω. From Fig. 8 an expression for ω can be derived (see Appendix C for details):

$$\omega = \frac{L_r \cdot \delta^*}{L_h \cdot \eta} \tag{31}$$

where L_r is the actual surface length of a roughness unit, L_h is that of a heterogeneity unit, and δ^* and η are the roughness and heterogeneity parameters, respectively:

$$\delta^* = \left(1 - \frac{1}{\delta^2}\right)^{1/4} \tag{32}$$

The value of δ^* changes from 0 to 1. For smooth surfaces, $\delta^*=0$. For extremely rough surfaces, $\delta^* \to 1$. For surfaces consisting of two materials, η is expressed by

$$\eta = \sqrt{|(\cos\theta_{e1} - \cos\theta_{e2})/2|} \tag{33}$$

The value of η also changes from 0 to 1. For a homogeneous surface, e.g., $\theta_{e1}=\theta_{e2}$, $\eta=0$. For extremely heterogeneous surfaces, e.g., $\theta_{e1}=0$ and $\theta_{e2}=180°$, $\eta=1$. For surfaces containing multiple materials (e.g. N materials), the heterogeneity parameter between the ith and the jth materials is defined as

$$\eta_{ij} = \sqrt{|(\cos\theta_{ei} - \cos\theta_{ej})/2|} \tag{34}$$

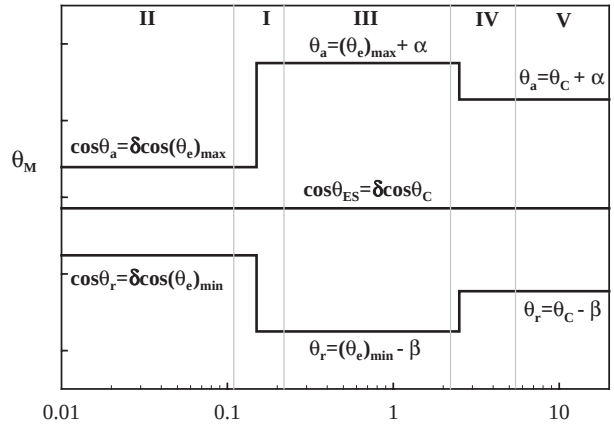

Fig. 9. The relationship between surface feature factor ω and surface classification. Region I: heterogeneity-dominated ($\omega<0.1$); Region III: mixed ($0.2<\omega<2$); Region V: roughness-dominated ($\omega>5$). Regions II and IV are two transit regions. The advancing, receding and system equilibrium contact angles are given for Regions I, III and V.

and then the average heterogeneity parameter of the surface is given by

$$\eta = \frac{1}{N}\sum_{i=1}^{N} \eta_{i,i+1} \tag{35}$$

where i means the ith material ($i=1,2,\ldots,N$), and $N+1$ represents the first material ($i=1$).

The value of ω could change from 0 to $\propto$. For smooth surfaces, $\omega=0$ whereas $\omega=\infty$ for homogeneous surfaces. By a great number of calculations for different values of ω and for different surface configurations, the relationship between the surface feature factor, ω, and surface classification, is found and shown in Fig. 9. This figure shows that surfaces can be divided into three major categories: heterogeneity-dominated surfaces (area I with $\omega<0.1$), mixed rough-heterogeneous surfaces (area III with $0.2<\omega<2$), and roughness-dominated surfaces (area V with $\omega>5$). With each of the three categories, the advancing, receding and system equilibrium contact angles can be obtained. Between the three categories, there are two transition regions (II and IV). In these two regions, the advancing and the receding contact angles are not easy to be determined. We tend to consider that they satisfy the equations in area III. Fig. 10 also shows that the system equilibrium contact angles can be expressed by the same equation for all surfaces.

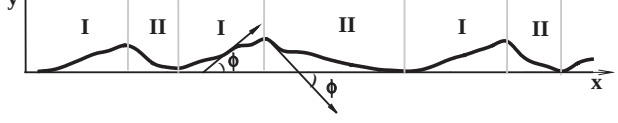

Fig. 10. A schematic illustration of a mixed surface, which may has an irregular topography. "I" represents the surface segments that have a positive tilt angle ($0° \le \phi \le 180°$). "II" indicates the segments that have a negative tilt angle ($-180° \le \phi < 0°$). The tilt angle is defined as the angle formed by the tangent at x and the x-axis.

7. Irregular surfaces

To analyze more general surface configurations than the above regular model surface (Fig. 2), an irregular surface, e.g., the one in Fig. 10, can be employed. The height at any point of the irregular surface, y, is a function of x and can still be generally described by Eq. (5). However, $y(x)$ can be any form of function so that it can represent an arbitrary surface configuration. For surface heterogeneity, the intrinsic contact angle may change at any surface spot, and can be described as a function of x with the form of Eq. (4).

For such an irregular surface as shown in Fig. 10, the tilt angle, ϕ, of the surface spot at point x, is defined as the angle formed by the tangent and the horizontal x-axis at x. For the surface segments indicated by "I", the tilt angle is in the positive range of 0° to 180°; for these segments indicated by "II", it has a negative value in the range from −180° to 0°.

7.1. Roughness-dominated irregular surfaces

For roughness-dominated irregular surfaces, Eq. (19) can be used. As dy/dx represents the slope of the surface profile at x, suppose the tilt angle is ϕ at this point, then

$$\frac{dy}{dx} = \tan\phi \tag{36}$$

Mathematically, the increment of surface length, ds, in Eq. (19) satisfies $(ds)^2=(dx)^2+(dy)^2$. Combining this relation with the above equation gives

$$\frac{ds}{dx} = \frac{1}{\cos\phi} \tag{37}$$

Substituting Eqs. (36) and (37) into (19) and setting $d\Delta F/dx=0$, the following expression can be obtained

$$\theta_M = \theta_C - \phi \tag{38}$$

The above equation shows that when the tilt angle has a smallest value (ϕ_{min}), the corresponding contact angle will be the largest. The smallest tilt angle can be obtained from the surface segments "II" and should be a negative value. This largest contact angle represents the advancing contact angle:

$$\theta_a = \theta_C - \phi_{min} \tag{39}$$

The above equation shows that for a roughness-dominated irregular surface, the advancing contact angle is determined by the smallest tilt angle of the surface and the Cassie contact angle.

Similarly, when the tilt angle has a largest value (ϕ_{max}), the corresponding contact angle will be the smallest. The smallest tilt angle can be obtained from the surface segments "I" and have a positive value. Then, receding contact angle can be expressed by

$$\theta_r = \theta_C - \phi_{max} \tag{40}$$

which shows that the receding contact angle is determined by the maximum tilt angle of the surface and the Cassie contact angle. Eqs. (39) and (40) will become the same as Eqs. (21) and (22) for the surface configuration shown in Fig. 2. From Eqs. (39) and (40), the contact angle hysteresis can be expressed by

$$\Delta\theta_H = \phi_{max} - \phi_{min} \tag{41}$$

This equation indicates that for roughness-dominated irregular surfaces, contact angle hysteresis is only determined by the surface topography (the maximum and minimum tilt angles) but independent of surface heterogeneity.

7.2. Heterogeneity-dominated irregular surfaces

For heterogeneity-dominated irregular surfaces, although Eqs. (25) and (26) were derived on the basis of the model surface that contains only two alternating materials strips, they can be applied to surfaces with any number of different material strips. The derivation is the same as that in Section 4. Contact angle hysteresis for heterogeneity-dominated irregular surfaces can then be obtained as

$$\Delta\theta_H = \arccos\left(\delta\cos(\theta_e)_{max}\right) - \arccos\left(\delta\cos(\theta_e)_{min}\right) \tag{42}$$

which shows that the contact angle hysteresis is determined by the maximum and minimum intrinsic contact angles as well as the surface roughness factor. In this case, the surface tilt angles, i.e., ϕ, do not have a direct effect on the contact angle hysteresis.

7.3. Mixed rough-heterogeneous irregular surfaces

For mixed rough-heterogeneous irregular surfaces, combining Eq. (30) with Eqs. (4) and (5) and setting $d\Delta F/dx=0$ give

$$\theta_M = \theta_e - \phi. \tag{43}$$

When θ_e has its maximum, $(\theta_e)_{max}$, and ϕ its smallest value, ϕ_{min}, θ_M will have a maximum value:

$$\theta_{max} = (\theta_e)_{max} - \phi_{min} \tag{44}$$

However, because for a mixed rough-heterogeneous irregular surface, $(\theta_e)_{max}$ and ϕ_{min} may not appear at the same surface spot, this θ_{max} may not exist. Therefore, it only represents the upper limit of possible contact angles. The advancing contact angle, θ_a, is equal to or smaller than θ_{max}.

Similarly, when θ_e has a minimum, $(\theta_e)_{min}$, and ϕ has a largest value, ϕ_{max}, θ_M will have a minimum value:

$$\theta_{min} = (\theta_e)_{min} - \phi_{max} \tag{45}$$

θ_{min} will represent the lower limit of possible contact angles, rather than the receding contact angle because $(\theta_e)_{min}$ and ϕ_{max} may not appear at the same surface spot. The receding contact angle, θ_r, is equal to or larger than θ_{min}.

With Eqs. (44) and (45), the upper limit of the contact angle hysteresis for mixed rough-heterogeneous irregular surfaces can be obtained

$$\Delta\theta_{H,max} = (\theta_e)_{max} - (\theta_e)_{min} + \phi_{max} - \phi_{min}. \quad (46)$$

This equation shows that both the maximum and minimum intrinsic contact angles and the surface topography will determine the upper limit of the contact angle hysteresis.

8. Comparison with experimental results

Miller et al. [32] measured the advancing and receding contact angles of water on vacuum-deposited polytetralfluroethylene (PTFE) thin films using a sessile drop method. The advancing contact angle they obtained on a film (deposited on a glass plate) is 146°. They also used atomic force microscopy (AFM) to image the surface and found that the surface was rough (mean roughness R_a=83.6 nm). The tilt angle (ϕ) of the surface obtained by a section analysis on the image was 50°. Such a surface can be considered as a rough but homogeneous surface. Eq. (39), $\theta_a=\theta_C-\phi_{min}$, should be applicable where the Cassie contact angle equals the intrinsic angle (θ_e) of the PTFE film, which is 95° [33], and ϕ_{min} is equal to −50°. Thus, we obtain $\theta_a=\theta_C-\phi_{min}=\theta_e+\phi=145\approx146°$ (measured value). This indicates the prediction from Eq. (39) agrees with the measured value.

The receding contact angle that Miller et al. [32] obtained on the PTFE surface is 60°. They found that the previous theories [2,3,7–9] did not provide a good prediction on the receding contact angle. Using symmetric roughness peaks, these theories obtained $\theta_r=\theta_e-\phi=45°$. However, the present study shows that the advancing and receding contact angles are determined by different tilt angles (see Eqs. (39) and (40)). Because of the possible asymmetry of the surface, the tilt angle, 50°, that they obtained on one side of the peak, may not be applicable to the receding angle. From Eq. (40), $\theta_r=\theta_C-\phi_{max}$, we estimated that the tilt angle on the other side of the peak could be $\phi_{max}=\theta_e-\theta_r=95-60=35°$ if the peaks are indeed unsymmetrical. This shows that our model provides a possibility to explain the measured receding contact angle.

Katoh et al. [34] measured the advancing and receding contact angles of water and ethanol–water solutions on a series of surfaces with regular grooves (see the inset of Fig. 11). The results of both advancing and receding contact angles as a function of the groove angle, ϕ, are presented in Fig. 11. Their experimental results showed that θ_a (θ_r) increased (decreased) linearly with ϕ. To fit the results, they employed the following relations [6,9]: $\theta_a=\theta_e+\phi$ and $\theta_r=\theta_e-\phi$ for advancing and receding contact angles. These two equations give $\theta_a=\theta_r$ if the surfaces were smooth, i.e., $\phi=0°$. However, by extrapolating the results to $\phi=0°$, they found that $\theta_a\neq\theta_r$. Then they modified these two equations with a parameter β: $\theta_a=\theta_e+\phi+\beta$ and

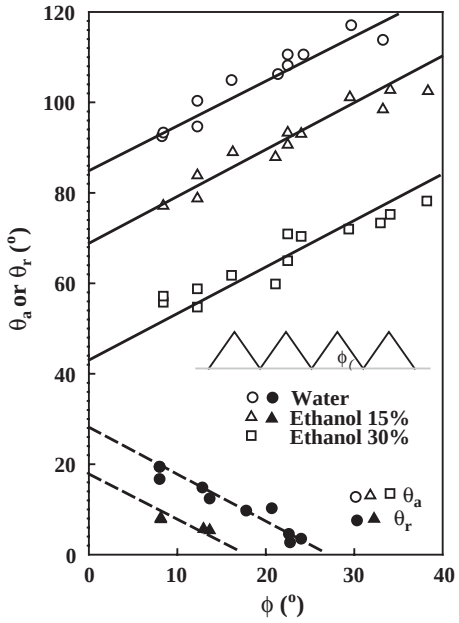

Fig. 11. Comparison between the theoretical predictions (lines) and the experimental results (symbols) of Katoh et al. [34]. The surface configuration is shown in the inset. It consists of regular grooves with a tilt angle, ϕ. Open symbols: advancing contact angle. Filled symbols: receding contact angle. Solid lines: advancing contact angles obtained from Eq. (39). Dotted lines: receding contact angles obtained from Eq. (40).

$\theta_r=\theta_e-\phi-\beta$ for advancing and receding contact angles, respectively. Here β represents the effect of the so-called "infinitesimal roughness" [34]. A problem arises from their modification: as β was only a property of the surface, it should be independent of the liquids used to measure the contact angles. However, they obtained different values of β for different liquids.

To explain this situation, the surface could be considered to be heterogeneous. Such heterogeneity may result from the orientation and/or physical status of the surface molecules. Thus, the surface can be treated as a mixed rough-heterogeneous surface. As a result, the advancing and receding contact angles can be expressed by

$$\theta_a = \theta_{max} = r_{max} - \phi_{min} = (\theta_e)_{max} + \phi \quad (47)$$

$$\theta_r = \theta_{min} = (\theta_e)_{min} - \phi_{max} = (\theta_e)_{min} - \phi \quad (48)$$

For smooth but heterogeneous surfaces ($\phi=0$), these two equations can be reduced to $\theta_a=(\theta_e)_{max}$ and $\theta_r=(\theta_e)_{min}$. Thus, we can obtain $\theta_a\neq\theta_r$ at $\phi=0$. In fact, if we suppose $(\theta_e)_{max}=\theta_e+\beta$ and $(\theta_e)_{min}=\theta_e-\beta$, our Eqs. (47) and (48) will become the same as the expressions suggested by Katoh et al. [34]. However, here β will not represent the effect of the "infinitesimal roughness". Instead, it represents the change of intrinsic contact angle due to the surface heterogeneity. Consequently, β is dependent on the liquid used. This is consistent with the experimental results. Thus, our explanation seems more reasonable than the modification based on the effect of the "infinitesimal roughness".

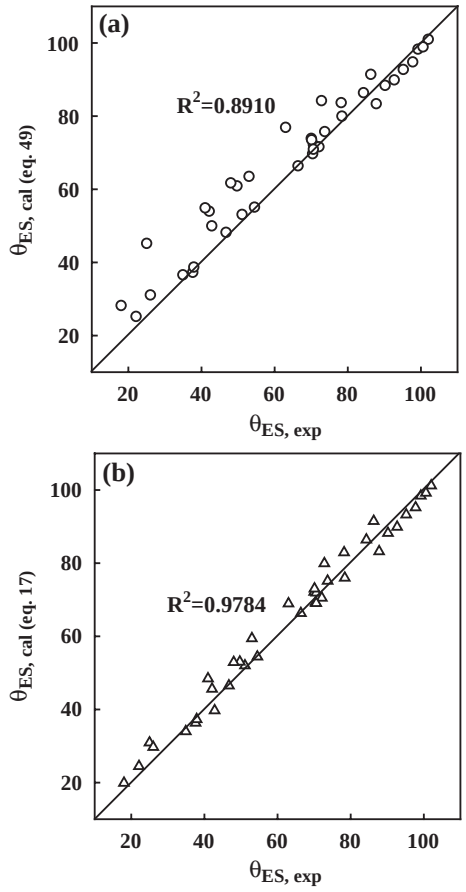

Fig. 12. Comparison of measured system equilibrium contact angles with the calculated values. (a) Eq. (49) was used. (b) Eq. (17) was used.

However, it cannot be excluded that the adsorption of the solution on the surface and/or other unknown factors may play a role in the observed inconsistence.

Eqs. (47) and (48) can be used to fit the data in Fig. 11. The lines in Fig. 11 gives $(\theta_e)_{max}$ and $(\theta_e)_{min}$: 86° and 27° for water, 69° and 17° for ethanol–water solution (15%), and 27° and 0° for ethanol–water solution (30%). Thus, the advancing and receding contact angles can be expressed by, e. g., $\theta_a = 86 + \phi$ and $\theta_r = 27 - \phi$ for water. Fig. 11 shows that the theoretical predictions from Eqs. (47) and (48) agree well with the experimental results.

The third experimental comparison is related to system equilibrium contact angles, which can be generally expressed as a function of surface roughness factor and the Cassie contact angle by from Eq. (17). However, in the literature, the following relation was used to calculate the system equilibrium contact angles [35–38]:

$$\cos\theta_{ES} = \frac{\cos\theta_A + \cos\theta_r}{2} \tag{49}$$

From the quantitative analyses of advancing/receding contact angles, such a relation cannot be derived. However, the above equation, or even a simpler expression [34]

$$\theta_{ES} = (\theta_A + \theta_r)/2 \tag{50}$$

has been used to calculate the system equilibrium contact angle. Eqs. (49) and (50) are empirical relations at best.

Della Volpe et al. [37,38] developed a simple experimental device to measure system equilibrium angles. Andrieu et al. [36] also measured the system equilibrium angles on various surfaces. By modeling the surfaces, these researchers studied roughness-dominated surfaces with isosceles triangles, the advancing and receding contact angles can be expressed as

$$\theta_a = \theta_C + \phi \tag{51}$$

$$\theta_r = \theta_C - \phi \tag{52}$$

where ϕ denotes the surface tilt angle, from which the surface roughness factor can be obtained: $\delta = 1/\cos\phi$. From the experimental results of advancing and receding contact angles, θ_C and δ can be obtained with the above two equations. Then, with Eq. (17), the system equilibrium contact angle can be calculated.

Comparing the experimental results of θ_{ES} with the predicted values from Eqs. (49) and (50) shows that θ_{ES} from Eq. (17) agrees with $\theta_{ES,\,exp}$ better than that from Eq. (49) (see Fig. 12). In Fig. 12b all points are in a very narrow region around the bisecting line, with a R-squared value (R^2) of 0.9784 and an average error of 5.36% ($\frac{1}{N}\sum\frac{|\theta_{ES,exp}-\theta_{ES,cal}|}{\theta_{ES,exp}}$). This indicates that the results from Eq. (17) are in a good agreement with the experimental results. Comparatively, the points in Fig. 12a are much more scattered with $R^2 = 0.8910$ and an average error of 11.26%.

9. Conclusions

This paper presents a preliminary study of the thermodynamics of contact angles on rough, heterogeneous surfaces. The following conclusions can be drawn:

Rough, heterogeneous surfaces were successfully modelled by considering a two-dimensional regular model surface containing trapezoidal bumps and alternating material strips. This model surface was further extended to irregular surfaces. Advancing, receding and system equilibrium contact angles were quantitatively correlated to surface topography, roughness and heterogeneity. The contact angles theoretically predicted by these quantitative relations agree well with the experimental results found in the literature. To our best knowledge, this is the first thermodynamic modelling of contact angles on rough and heterogeneous surfaces.

A parameter named surface feature factor (ω) was defined to classify surfaces into three categories: roughness-dominated, heterogeneity-dominated and mixed-rough-heterogeneous. For roughness-dominated surfaces, contact angle hysteresis is independent of surface intrinsic contact angles but determined by the maximum and minimum surface tilt angles: $\Delta\theta_H = \phi_{max} - \phi_{min}$. For heterogeneity-

dominated surfaces, contact angle hysteresis is determined by the surface roughness factor and the maximum and minimum intrinsic contact angles: $\Delta\theta_H = \arccos(\delta\cos(\theta_e)_{max}) - \arccos(\delta\cos(\theta_e)_{min})$. For mixed rough-heterogeneous surfaces, both surface topography and heterogeneity contribute to the upper limit of contact angle hysteresis: $\Delta\theta_{H,\ max} = (\theta_e)_{max} - (\theta_e)_{min} + \phi_{max} - \phi_{min}$. These statements are true for both regular and irregular surfaces.

System equilibrium contact angles, θ_{ES}, are independent of surface categories and can always be expressed by $\cos\theta_{ES} = \delta\cos\theta_C$. This expression can be reduced to $\theta_{ES} = \theta_W$ (the Wenzel contact angle) for rough but homogeneous surfaces, and $\theta_{ES} = \theta_C$ (the Cassie contact angle) for heterogeneous but smooth surfaces.

Nomenclature

a_1, a_2	surface area fraction of material 1, 2 such that $a_1 + a_2 = 1$
b	length of the smooth portion of a repeat unit in Fig. 1
c	length of the top side of a trapezoidal bump in Fig. 1
h_0	height of a trapezoidal bump in Fig. 1
H	length of a liquid front
H_0	length of a liquid front at the reference state
l	planar length of a repeated roughness unit containing a trapezoidal bump in Fig. 1
L	liquid front width
L_h	length of a heterogeneity unit
L_r	non-planar length of a roughness unit,
N	number of surface materials
s	non-planar length variable of a rough surface
S_{abc}	area of the triangle abc in Fig. 8
S_{ABC}	area of the triangle ABC in Fig. 8
x	horizontal coordinate
y	vertical coordinate
w_1, w_2	width of material strip 1, 2
θ_a	advancing contact angle
θ_C	Cassie contact angle
θ_e	intrinsic contact angle
θ_{ES}	system equilibrium contact angles
θ_M	macroscopic/apparent contact angle
θ_r	receding contact angle
θ_W	Wenzel contact angle
θ_Y	Young contact angle
$(\theta_e)_{max}$	Maximum intrinsic contact angle
$(\theta_e)_{min}$	Minimum intrinsic contact angle
ϕ	Surface tilt angle formed by the tangent at surface spot x and the x-axis
γ_{lv}	surface tension of a liquid
γ_{sl}	interfacial tension between a solid and a liquid
γ_{sv}	interfacial tension between a solid and a gas
δ	roughness factor: the ratio of the actual surface area to the corresponding geometrically projected area
α, β	geometric angles of the trapezoid in Fig. 1
ω	surface feature factor
δ^*	roughness parameter
η	average heterogeneity parameter of a surface
η_{ij}	heterogeneity parameter between materials i and j
ΔF	free energy change of a system
ΔF_1	free energy change due to a change in solid–vapor and solid–liquid interfacial areas
ΔF_2	free energy change due to a change in liquid–vapor interfacial area.

Acknowledgements

Financial support from the Natural Sciences and Engineering Research Council of Canada (NSERC), Canadian Foundation for Innovation (CFI), Ontario Graduate Scholarships in Science and Technology (OGSST), the Premier's Research Excellent Award, and the Canada Research Chairs program is gratefully acknowledged.

Appendix A. Validation of the model

To validate our model, the free energy curves for several specific model surfaces were obtained. These surfaces included the ideal smooth and homogeneous surface, the idealized rough but homogeneous surface, and the idealized heterogeneous but smooth surface. The results were compared with the results obtained by Neumann and coworkers [2,3,9].

A.1. Ideal smooth and homogenous surfaces

When we set $\theta_{e1} = \theta_{e2}$ and $\alpha = \beta = 0$, the model surface in Fig. 1 becomes a smooth and homogeneous surface, which has been conventionally identified as an ideal surface. For such an ideal surface, the Young equation should be satisfied and there exists only one contact angle, which is the Young equilibrium contact angle, or the intrinsic contact angle of the system. By rewriting Eqs. (9) and (10) for such an ideal surface, we obtain

$$\Delta F = -L\gamma_{lv}\cos\theta_e x + L\gamma_{lv}\left(\sqrt{H_0^2 + x^2} - H_0\right) \qquad (A1-1)$$

$$\tan\theta_M = \frac{H_0}{x} \qquad (A1-2)$$

From the above two equations, the free energy change of the entire system, ΔF, as a function of the macroscopic contact angle, θ_M, can be computed. For these calculations, we set $H_0 = 1200$ μm. A series of plots of ΔF versus θ_M with different θ_e are shown in Fig. A1-1. From this figure, it can be seen that each plot is a smooth curve with a minimum ΔF point. The minimum is at $\theta_M = \theta_e$. These plots indicate that for an ideal surface there is only one stable contact angle,

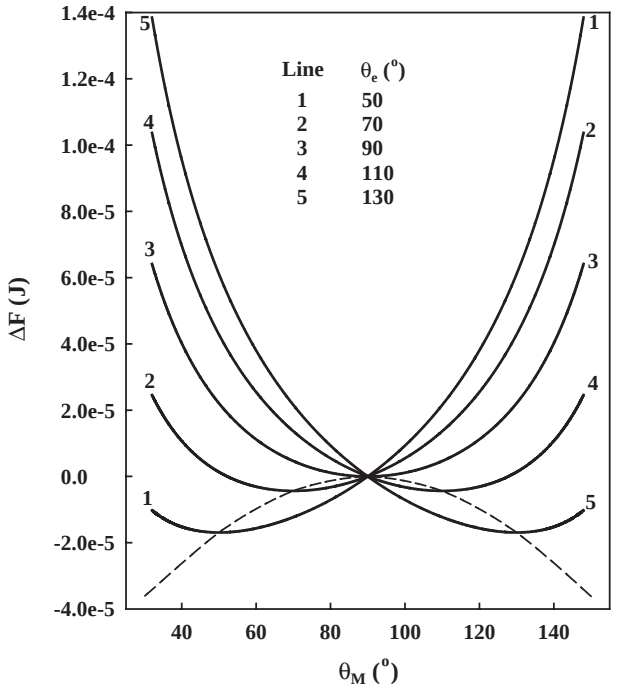

Fig. A1-1. Free energy curves for ideal smooth, homogeneous surfaces. The dashed line connects all the minima.

the intrinsic or Young equilibrium contact angle. The minimum ΔF point, in fact, can be directly obtained by taking the derivative of ΔF from Eq. (9):

$$\frac{d\Delta F}{dx} = -L\gamma_{lv}\cos\theta_e + L\gamma_{lv}\frac{x}{\sqrt{H_0^2+x^2}} = -L\gamma_{lv}\cos\theta_e + L\gamma_{lv}\cos\theta_M \quad (A1-3)$$

At the minimum point, $d\Delta F/dx=0$, we obtain $\theta_M=\theta_e$. This result shows that the model is valid for ideal surfaces. Similar plots of free energy change for such ideal surfaces were obtained by Eick et al. [9].

A.2. Idealized rough but homogeneous surface

As stated in the Introduction section, the idealized rough but homogeneous surface proposed by Eick et al. [9] consists of isosceles triangles. In order to have the same surface configuration, we can set $\alpha=\beta$ and $c=b=0$ in our model surface. This surface configuration is shown in Fig. 3 (a). To compare our results with those of Eick et al. [9], we set $\alpha=\beta=45°$, $h_0=100$ μm, and $\theta_e=70°$. These settings are the same as those used in Fig. 14 of Ref. [2]. The results of free energy change as a function of macroscopic contact angle are shown in Fig. A1-2. This free energy curve is similar to that of Fig. 14 in Ref. [2]. From Fig. A1-2, we note that there exist many metastable states for such an idealized rough surface. From left to right, the first metastable state occurs at $\theta_M=25°$ and the last occurs at $\theta_M=115°$. These two contact angles are the minimum and the maximum of the possible contact angles of the system, which correspond to the receding and the advancing contact angles, $\theta_r=25°$ and $\theta_a=115°$, respectively. In addition, from the values of the advancing and receding contact angle we find that the advancing and receding contact angles are related to the geometry of the surface and the intrinsic contact angle of the system:

$$\theta_a = \theta_e + \alpha \quad (A1-4)$$

$$\theta_r = \theta_e + \alpha \quad (A1-5)$$

By setting $d\Delta F/dx=0$, we can obtain the above two relations from our model equations as follows. Rewriting Eq. (9) for the idealized rough surface, we obtain

$$\Delta F = -L\gamma_{lv}\cos\theta_e\frac{x}{\cos\alpha} + L\gamma_{lv}\left(\sqrt{(H_0-y)^2+x^2}-H_0\right) \quad (A1-6)$$

and then

$$\frac{d\Delta F}{dx} = -L\gamma_{lv}\cos\theta_e\frac{1}{\cos\alpha} - L\gamma_{lv}\sin\theta_M\frac{dy}{dx} + L\gamma_{lv}\cos\theta_M \quad (A1-7)$$

There are two possible values for dy/dx, either $\tan\alpha$ or $-\tan\alpha$. By satisfying $d\Delta F/dx=0$, we can obtain Eqs. (A1-4) and (A1-5) from Eq. (A1-7).

Another point that we note from the curve in Fig. A1-2 is that the system exhibits a global minimum, which represents the system equilibrium contact angle, θ_{ES}. The value of θ_{ES} is approximate/equal to the Wenzel contact angle of the system, θ_W. It has been mathematically proven [13] that the θ_W becomes an excellent approximation to the θ_{ES} when the size of the drop becomes very large

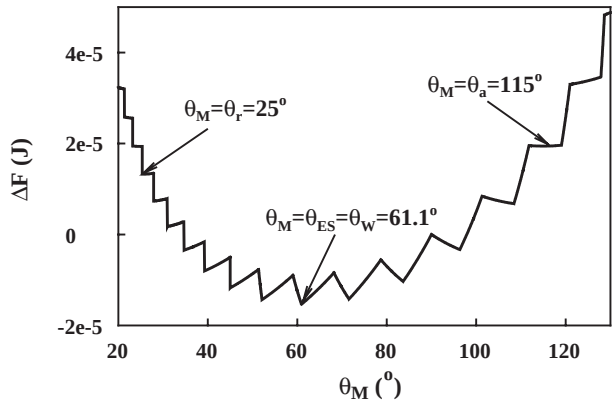

Fig. A1-2. Free energy curve for an ideal rough but homogeneous surface, which consists of isosceles triangular peaks with $l=200$ μm, $c=b=0$, $\alpha=\beta=45°$, $\theta_e=70°$, and $H_0=1000$ μm. (the same surface configuration as used in Fig. 14 of Ref [2]).

compared with the scale of roughness. This conclusion can also be proved by our model. When H_0 is large enough compared with roughness scale, Eqs. (A1-1)–(A1-6) can be approximated as:

$$\Delta F = -L\gamma_{lv}\cos\theta_e \frac{x}{\cos\beta} + L\gamma_{lv}\left(\sqrt{H_0^2 + x^2} - H_0\right) \quad (A1-8)$$

Differentiating the above equation and applying $d\Delta F/dx=0$ at the global minimum point, we obtain

$$\cos\theta_M = \cos\theta_{ES} = \delta\cos\theta_e \quad (A1-9)$$

Comparing the above equation with the Wenzel equation, we obtain $\theta_{ES}=\theta_W$.

A.3. Idealized heterogeneous but smooth surface

If we set $\alpha=\beta=0°$, the model surface in Fig. 2 becomes an idealized heterogeneous but smooth surface. Such a heterogeneous surface consists of alternating materials strips of equal width. To compare our results with those of Eick et al. [9], we set $\theta_{e1}=40°$, $\theta_{e2}=30°$, strip width $w_1=w_2=100$ μm, and $H_0=1400$ μm. The free energy change of the system is shown in Fig. A1-3. The free energy curve is similar to that of Eick et al. [9]. There are two points that should be noted from the curve. First, it exhibits a saw-tooth structure, which includes many local minimum points. Each local minimum represents a metastable state. Similar to that of an idealized rough surface, the first and the last metastable states will correspond to the receding and the advancing contact angles, 30° and 40°, respectively. Therefore, this curve predicts contact angle hysteresis. Second, it shows a global minimum point, at which the system reaches its equilibrium state with a contact angle $\theta_{ES}=34.35°$. This system equilibrium contact angle is close to the Cassie contact angle of the system, θ_C (=35.31°).

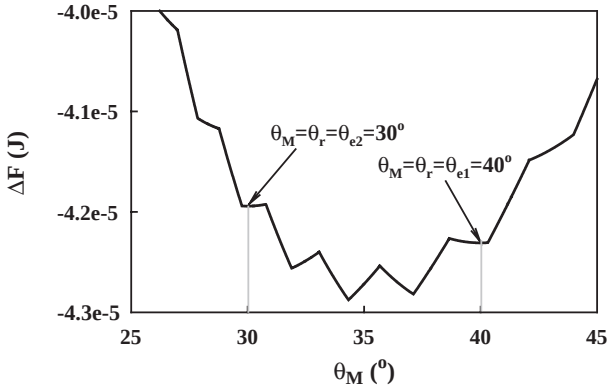

Fig. A1-3. Free energy curves for an ideal smooth but heterogeneous surface, which consists of alternating material strips with $\theta_{e1}=40°$, $\theta_{e2}=30°$, $w_1=w_2=100$ μm, and $H_0=1400$ μm. (the same surface configuration as used in Fig. 3 of Ref [2]).

Mathematically, we can obtain the advancing, the receding, and the system equilibrium contact angles directly from our model equations for such an idealized heterogeneous surface. In this case, Eq. (14) can be replaced by Eq. (A1-2) and Eq. (9) can be simplified as

$$\Delta F = \int_0^x -L\gamma_{lv}\cos\theta_e(x)dx + L\gamma_{lv}\left(\sqrt{H_0^2 + X^2} - H_0\right) \quad (A1-10)$$

The derivative of ΔF can be expressed by

$$\frac{d\Delta F}{dx} = -L\gamma_{lv}\cos\theta_e(x) + L\gamma_{lv}\cos\theta_M \quad (A1-11)$$

The system has two intrinsic contact angles, θ_{e1} and θ_{e2}. At the first and the last local minimum points, $d\Delta F/dx=0$ must be satisfied. From Eq. (A1-11), we will obtain either $\theta_M=\theta_{e1}$ or $\theta_M=\theta_{e2}$. These two angles represent the advancing and receding contact angles.When H_0 is great enough, combining with Cassie equation, we can approximate Eq. (A1-10) as

$$\Delta F = -L\gamma_{lv}\cos\theta_c x + L\gamma_{lv}\left(\sqrt{H_0^2 + x^2} - H_0\right) \quad (A1-12)$$

By differentiating the above equation and applying $d\Delta F/dx=0$ at the global minimum point, we obtained $\theta_{ES}=\theta_C$.

From the above discussion, we conclude that our model is as efficient as the existing model for these specific surfaces.

Appendix B. Effect of the Liquid Front Length (H_0)

To what extent the assumption of liquid front is still valid when considering the characteristic size of surface roughness and/or heterogeneity? In this appendix, we try to answer this question and present the results showing the effect of the liquid front length (H_0).

Fig. A2-1 shows the free energy curves obtained at different values of H_0. For the same idealized rough but homogeneous surface as used in Fig. A1-2, which contains isosceles triangles with a width of 200 μm, three free energy curves were obtained at $H_0=500$, 1000, and 2000 μm, respectively. The three curves are shown in Fig. A2-1(a), from which one can see that all the advancing contact angles are the same (115°) while all the receding contact angles equal 35°. The advancing and receding angles satisfy Eqs. (A1-4) and (A1-5), respectively. This indicates that the value of H_0 does not affect advancing and receding contact angles even when a value close to the size of the roughness peaks, e.g., 500 μm was used. However, the system equilibrium contact angle obtained at $H_0=500$ μm is 53°, far away from the predicted value of 61.1° by Eq. (A1-9). When larger H_0 was used, the system equilibrium contact angles obtained, 61° at $H_0=1000$ μm and 60° at $H_0=2000$ μm, are very close to the predicted value. This indicates that

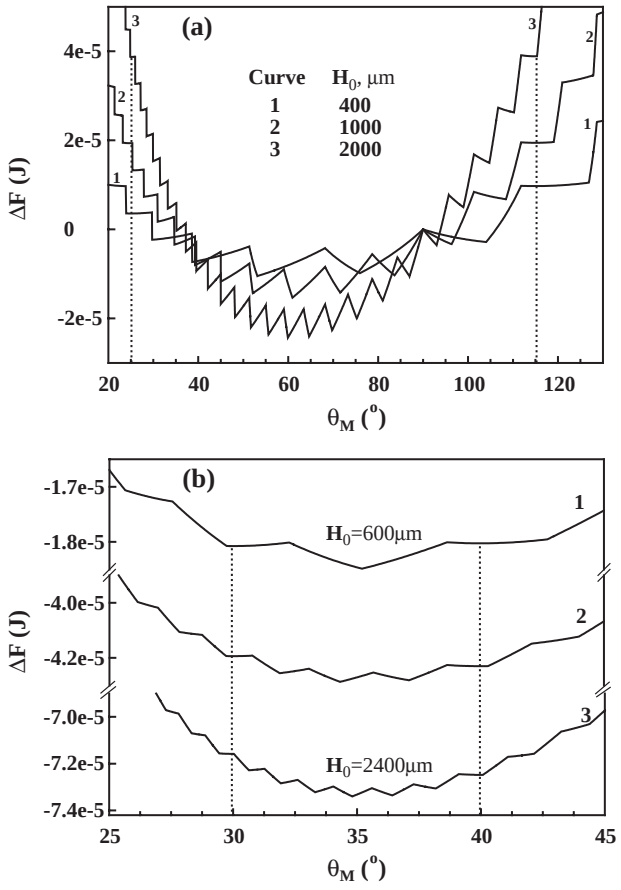

Fig. A2-1. Effect of H_0 on the calculation of free energy. (a) Free energy curves for the idealized rough but homogeneous surface used in Fig. A1-2. (b) Free energy curves for the idealized smooth but heterogeneous surface used in Fig. A1-3.

to obtain a system equilibrium contact angle close to the theoretical one, a value of H_0 much larger than the size of roughness peaks must be used.

Fig. A2-1(b) shows three free energy curves for the same idealized smooth but heterogeneous surface as used in Fig. A1-3. This surface contains two materials with $\theta_{e1}=40°$ and $\theta_{e2}=30°$ and strip width $w_1=w_2=100$ μm. Similar to the case of Fig. A2-1(1), the advancing and receding contact angles obtained are independent of the H_0 values used. The system equilibrium contact angles obtained are 35.2, 34.4, and 34.8° for $H_0=600$, 1400, 2400 μm, respectively. These values are all close to the Cassie contact angle, 35.3°. As θ_{e1} and θ_{e2} are quite close to each other, it is reasonable that the obtained equilibrium angles seem to be independent of the H_0 used. However, our calculations for other cases show that a larger H_0 must be used in order to obtained a equilibrium angle close to the theoretical one.

Appendix C. Derivation of the surface feature factor

As shown in Fig. 8, the area of triangle ABC, S_{ABC}, which represents the "sum" of free energy ΔF_2 for the liquid front to move over a peak due to net roughness effect, can be expressed by

$$\begin{aligned} S_{ABC} &= -\int_0^{x1}\left(\sqrt{(H_0-y)^2+x^2}-H_0\right)dx \\ &\approx -h\cos\beta\cdot\left(\sqrt{(H_0-h\sin\beta)^2+(h\cos\beta)^2}-H_0\right) \\ &= -h\cos\beta\cdot H_0\left(\sqrt{1-\frac{2h\sin\beta}{H_0}+\left(\frac{h}{H_0}\right)^2}-1\right) \\ &\approx -h\cos\beta\cdot H_0\left(1-\frac{1}{2}\cdot\frac{2h\sin\beta}{H_0}-1\right) \\ &= h^2\cos\beta\sin\beta \end{aligned} \qquad (A2-1)$$

where $x1$ is the projected length of a roughness unit in the axis of x and h is the length of the side of the triangle.

Similarly, to calculate the area of triangle abc S_{abc}, in Fig. 8, which represents the "sum" of free energy term, ΔF_1, for the liquid front to move over a heterogeneity unit, we can shift the co-ordinate so that at point a, $s=0$, and then S_{abc} can be expressed by

$$\begin{aligned} S_{abc} &= \int_0^{x2}\left(\int_0^{s}-\cos\theta_e(x)ds\right)dx \\ &\quad -\int_0^{x2}\left(-\frac{\cos\theta_{e1}W_1+\cos\theta_{e2}W_2}{\cos\beta(w_1+w_2)}\right)dx \\ &= S(1)+S(2) \end{aligned} \qquad (A2-2)$$

where $x2$ is the projected length of a heterogeneity unit in the axis of x, and $S(1)$ and $S(2)$ are the first and second integration items, respectively. $S(1)$ and $S(2)$ can be obtained by

$$\begin{aligned} S(1) &= -\int_0^{w_1\cos\beta}\cos\theta_{e1}\frac{x}{\cos\beta}dx-\int_{w_1\cos\beta}^{(w_1+w_2)\cos\beta} \\ &\quad\times\left[w_1\cos\theta_{e1}+\cos\theta_{e2}\left(\frac{x}{\cos\beta}-w_1\right)\right] \\ dx &= -\frac{\cos\beta}{2}\left(\cos\theta_{e1}w_1^2+\cos\theta_{e2}w_2^2+2\cos\theta_{e1}w_1w_2\right) \end{aligned} \qquad (A2-3)$$

$$\begin{aligned} S(2) &= \int_0^{(w_1+w_2)\cos\beta}\left(\frac{\cos\theta_{e1}w_1+\cos\theta_{e2}w_2}{\cos\beta(w_1+w_2)}x\right)dx \\ &= \frac{\cos\beta}{2}\left(\cos\theta_{e1}w_1^2+\cos\theta_{e2}w_2^2+(\cos\theta_{e1}+\cos\theta_{e2})w_1w_2\right) \end{aligned} \qquad (A2-4)$$

Substitute the above two equations into Eq. (A2-2), we obtain

$$S_{abc}=\frac{\cos\beta(\cos\theta_{e2}-\cos\theta_{e1})w_1w_2}{2} \qquad (A2-5)$$

If the two material strips have the same width, i.e., $w_1=w_2=w$, the above equation can be rewritten as

$$S_{abc} = \frac{\cos\beta(\cos\theta_{e2} - \cos\theta_{e1})w^2}{2} \qquad (A2-6)$$

Based on the definition of surface feature factor ω, using Eqs. (A2-1) and (A2-6), we obtain

$$\omega = \sqrt{\frac{S_{ABC}}{S_{abc}}} = \frac{h\cdot\sqrt{\sin\beta}}{w\cdot\sqrt{|(\cos\theta_{e1} - \cos\theta_{e2})/2|}}$$

$$= \frac{L_r(1-\cos^2\beta)^{1/4}}{L_h\cdot\sqrt{|(\cos\theta_{e1} - \cos\theta_{e2})/2|}} = \frac{L_r\cdot\delta^*}{L_h\cdot\eta} \qquad (A2-7)$$

where L_h is the length of a heterogeneous unit, e. g. w_1+w_2 ($w=L_h/2$), L_r is the non-planar length of a rough unit, e.g. for a isosceles triangle $L_r=2h$, δ^* is a roughness parameter, η is the heterogeneity factor of the two materials. δ^* and η can be respectively expressed by

$$\delta^* = \left(1 - \frac{1}{\delta^2}\right)^{1/4} \qquad (A2-8)$$

$$\eta = \sqrt{|(\cos\theta_{e1} - \cos\theta_{e2})/2|}. \qquad (A2-9)$$

References

[1] Young T. In: Peacock G, editor. Miscellaneous works, vol. 1. London: J. Murray; 1855.
[2] Li D, Neumann AW. In: Neumann AW, Spelt JK, editors. Applied surface thermodynamic. New York: Marcel Dekker, Inc.; 1996. Chapter 3.
[3] Neumann AW, Good RJ. J Colloid Interface Sci 1972;38:341.
[4] Wenzel RN. Ind Eng Chem 1936;28:988.
[5] Cassie BD. Disc Faraday Soc 1948;3:11.
[6] Shuttleworth R, Bailey GLJ. Disc Faraday Soc 1948;3:16.
[7] Johnson Jr RE, Dettre RH. J Phys Chem 1964;68:1744.
[8] Johnson Jr RE, Dettre RH. Adv Chem Ser 1964;43:112.
[9] Eick JD, Good RJ, Neumann AW. J Colloid Interface Sci 1975;53:235.
[10] Huh C, Mason SG. J Collod Interface Sci 1977;60:11.
[11] Oliver JF, Mason SG. J Mater Sci 1980;15:431.
[12] Joanny JF, de Gennes PG. J Chem Phys 1984;81:552.
[13] Robbins MO, Joanny JF. Europhys Lett 1987;3:729.
[14] Marmur A. J Colloid Interface Sci 1994;168:40.
[15] Brandon S, Marmur A. J Colloid Interface Sci 1996;183:351.
[16] Marmur A. Colloids Surf A Physicochem Eng Asp 1998;136:209.
[17] Marmur A. J Imaging Sci Technol 2000;44:406.
[18] Marmur A. Colloids Surf A Physicochem Eng Asp 1998;136:81.
[19] Extrand CW. Langmuir 2002;18:7991.
[20] Öpik U. J Colloid Interface Sci 2000;223:143.
[21] Lam CNC, Ko RHY, Yu LMY, Ng A, Li D, Hair ML, Neumann AW. J Colloid Interface Sci 2001;243:208.
[22] Lam CNC, Kim N, Hui D, Kwok DY, Hair ML, Neumann AW. Colloids Surf A Physicochem Eng Asp 2001;189:265.
[23] Lam CNC, Wu R, Li D, Hair ML, Neumann AW. Adv Colloid Interface Sci 2002;96:169.
[24] Chibowski E. Adv Colloid Interface Sci 2003;103:149.
[25] Decker EL, Frank B, Suo Y, Garoff S. Colloids Surf A Physicochem Eng Asp 1999;156:177.
[26] Guoin H. Contin Mech Thermodyn 2003;15:581.
[27] Guoin H. Contin Mech Thermodyn 2003;15:597.
[28] Chen YL, Helm CA, Israelachvili JN. J Phys Chem 1991;95:10736.
[29] Adamson AW, Gast AP. Physical chemistry of surfaces. 6th ed. New York: John Wiley and Sons, Inc.; 1997. p. 352–3.
[30] Gaydos J, Neumann AW. J Colloid Interface Sci 1987;120:76.
[31] Wolansky G, Marmur A. Langmuir 1998;14:5292.
[32] Miller JD, Veeramasuneni S, Drelich J, Yalamanchili MR, Yamauchi G. Polym Eng Sci 1996;36:1849.
[33] Busscher HJ, Van Pelt AWJ, De Boer P, De Jong HP, Arends J. Colloids Surf 1984;9:319–31.
[34] Katoh K, Fujita H, Yamamoto M. Nippon Kikai Gakkai Ronbunshu Bhen 1991;57:4124.
[35] Decker EL, Garoff S. J Adhes 1997;63:159.
[36] Andrieu C, Sykes C, Brochard F. Langmuir 1994;10:2077.
[37] Della Volpe C, Maniglio D, Marra M, Siboni S. Colloids Surf 2002;206:47.
[38] Della Volpe C, Maniglio D, Marra M, Siboni S. Oil Gas Sci Technol 2001;56:9.